JOIV : Int. J. Inform. Visualization, 8(3-2): IT for Global Goals: Building a Sustainable Tomorrow - November 2024 1938-1948

INTERNATIONAL JOURNAL ON INFORMATICS VISUALIZATION

journal homepage : www.joiv.org/index.php/joiv

An Innovative Approach for Improving Navigation Performance of Robust Land-Based Vehicles

Mostafa Ghouneem [a,*], Amr Wassal [a]

[a] *Computer Engineering Department, Cairo University, Giza, Egypt*

Corresponding author: [*]mostafamahmoud86@eng.cu.edu.eg

***Abstract*—The Extended Kalman Filter (EKF) stands as a prominent choice within navigation systems, particularly in scenarios involving the integration of a Reduced Inertial Sensor System (RISS) with the Global Positioning System (GPS). However, despite its widespread adoption, the EKF grapples with many challenges, including the propensity to underestimate filter uncertainties, contend with unreliable GPS signals, and confront errors stemming from linearization processes. These issues invariably contribute to a decline in overall system performance. Considering these challenges, this paper endeavors to introduce a groundbreaking integration algorithm to mitigate the inherent shortcomings of the EKF. The proposed algorithm employs innovative strategies to address these challenges comprehensively. Firstly, it incorporates a dynamic self-tuning mechanism meticulously designed to improve filter configuration in real-time, ensuring adaptability to varying operating conditions. The algorithm also integrates a meticulously engineered GPS Integrity algorithm to filter out mistaken readings and bolster the reliability of the navigation solution. Furthermore, the algorithm adopts the Unscented Kalman Filter (UKF), renowned for handling non-linearities directly, thereby cutting the need for the cumbersome linearization procedures inherent in the EKF. Comparative evaluations against the traditional EKF method prove the effectiveness of the proposed approach. Significant performance enhancements are evident using two datasets from a VTI SCC1300-D04 IMU unit compared to high-precision Novatel SPAN ground truth data. These improvements are quantified through RMSE analysis, showing substantial strides in navigation accuracy. Overall, the results underscore the transformative potential of the proposed integration algorithm in advancing navigation system capabilities.**

***Keywords*—Navigation system; reduce inertial sensor system; inertial navigation systems; global positioning system.**

Manuscript received 18 Mar. 2024; revised 14 Apr. 2024; accepted 9 May 2024. Date of publication 30 Nov. 2024.
International Journal on Informatics Visualization is licensed under a Creative Commons Attribution-Share Alike 4.0 International License.

I. INTRODUCTION

Inertial Navigation Systems (INS) track a vehicle's position, velocity, and orientation using accelerometers and gyroscopes (Inertial Measurement Units or IMUs) [1]. While correct for short periods, INS drift accumulates over time due to sensor errors and limitations in processing algorithms [2]. This problem is better with GPS or other aid sources. Specifically, accelerometer bias leads to position and velocity errors, gyroscopes cause errors in angles, and all errors grow with time [3]. Compared to traditional INS, RISS prioritizes cost, size, weight, and power consumption using fewer, lower-cost sensors [4]. This more straightforward design makes RISS less complex and more affordable. While sacrificing some short-term accuracy, RISS utilizes algorithms to estimate navigation states and finds applications in robotics, UAVs, smartphones, and even self-driving cars. While MEMS-based RISS offers good short-term accuracy, its long-term performance suffers due to sensor drift [5]. GPS, on the other hand, excels in long-term navigation but has limitations in accuracy and can be susceptible to signal outages. Combining RISS and GPS leverages their strengths for initial accuracy and long-term correction, leading to a more robust navigation system [6].

However, integrating these systems with the Extended Kalman Filter (EKF), a common technique for handling noisy and non-linear data [7], presents challenges. The EKF's dependence on linearization can affect accuracy, and precise tuning of filter parameters is crucial. Additionally, poor GPS data quality directly impacts EKF performance. These limitations can lead to system divergence, where filter estimates deviate significantly from the true state, ultimately hindering overall system performance [8]. The limitations of linearization in the EKF pave the way for the Unscented Kalman Filter (UKF) [9], [10]. UKF employs a deterministic sampling approach, working directly with the non-linear system. It selects a minimal set of sigma points representing

the system state, propagates them through the non-linearity, and accurately calculates the true mean and covariance (up to 3rd order) without linearization. While Table I highlights the advantages of UKF over EKF for RISS integration, UKF also has drawbacks. It can underestimate filter uncertainty and requires complex, time-consuming tuning procedures.

TABLE I
EXTENDED KALMAN FILTER VS UNSCENTED KALMAN FILTER FOR RISS

Feature	Extended Kalman Filter	Unscented Kalman Filter
Navigation State	Predict the error in the navigation state.	Predict the complete navigation state.
RISS non-linearity	Apply first-order approximation of the Taylor series expansion to linearize the RISS, resulting in a degradation of system accuracy.	Addressing the nonlinearity of the RISS system to enhance system accuracy.
Computation	Simple.	Complex.
Tuning	Require tuning for error covariance matrices, impacting the system's performance.	The system's performance is affected by the need to tune error covariance matrices and the additional parameters used to select the sigma points.
Convergence	Linearization may result in divergence in the RISS system.	Sigma points facilitate convergence in the RISS system.

Additionally, misleading GPS signals can still integrate mistaken data into the system. EKF-based integration of RISS and GPS for navigation systems faces challenges like linearization errors, filter tuning complexity, and sensitivity to unreliable GPS data. To address these shortcomings, a novel algorithm has been developed. This new approach tackles the issue of filter tuning by introducing a method specifically designed for RISS/GPS integration within the EKF framework. Additionally, it incorporates an algorithm to evaluate the quality of incoming GPS data and identify periods of GPS outages. This enhanced capability allows the system to distinguish between reliable and unreliable GPS measurements, improving overall robustness and filter performance.

Improving a Kalman filter ensures the best performance when estimating a system's state. The error covariance matrices within the system consist of the Q matrix, determining the error covariance of the driving information source (in this context, the RISS), the R matrix, determining the error covariance of the aiding information source (the GPS), and the P matrix, determining the error covariance of the system states [11]. The effectiveness of EKF-based RISS/GPS systems dramatically depends on the initial values of these error covariance matrices, influencing the accuracy of estimated states and the filter's convergence time [12]. The tuning process can be conducted manually or using algorithmic methods.

However, the tuning step is complex and time-consuming. Efforts to address the challenge of tuning Kalman Filters and their derivatives have been diverse. These initiatives aimed to estimate the initial values of covariance matrices like P, R, and Q, or dynamically adjust these values during operation to adapt to input characteristic changes. Powell [13] introduced an automated method to fine-tune the Extended Kalman Filter (EKF) using the Downhill Simplex Algorithm. The primary objective is to improve the EKF's precision in estimating the state of a dynamic system by adjusting key parameters, mainly covariance matrices.

Employing the Downhill Simplex Algorithm as a numerical optimization tool, the method minimizes a performance index based on state estimate errors. This automated tuning strategy seeks optimal values for filter parameters, enhancing data processing efficiency and state estimate accuracy. Powell's study likely demonstrates the practical applicability of the proposed technique through applications to numerical examples, showcasing its effectiveness in optimizing the EKF across various scenarios of increasing complexity. The fine-tuning of the error covariance matrix is traditionally carried out offline before filter execution.

Conversely, an adaptive filter dynamically adjusts its tuning parameters in real-time to enhance filter performance and minimize convergence time. 1976 Kenneth and Byron [14] proposed an adaptive filter for linear systems, utilizing empirical estimators. These estimators can concurrently estimate both the covariance matrix and bias associated with system model errors that adapt to unknown noise statistics. They assumed that the system noise exhibited slow variations while remaining stationary over N time steps to achieve an explicit maximum-likelihood estimator. In 2013, Matisko and Havlena introduced a novel tuning method for linear Kalman Filters (KF) [15]. Their approach utilized Bayesian principles and numerical techniques from the Monte Carlo group to estimate noise covariance matrices.

Through extensive simulations across diverse systems and settings, they demonstrated the effectiveness and consistency of the algorithms, particularly as the amount of data increased. The adaptive methodology Lee (2004) proposed is then applied to nonlinear systems. Lee [16] delves into an adaptive approach to Sigma Point Filtering for estimating state and parameter values. The method's adaptability involves dynamically adjusting filter parameters during runtime to improve the accuracy of state and parameter estimation. Lee introduces the adaptive unscented Kalman filter (AUKF) and the adaptive divided difference filter (ADDF).

The performance of both the AUKF and the ADDF surpasses that of standard nonlinear filters (EKF and UKF) in terms of rapid convergence and accurate estimation. In 2003, Bolognani et al. [17] investigated the tuning of the EKF in sensorless Permanent Magnet Synchronous Motor (PMSM) drives. The primary focus was optimizing the EKF for sensorless control applications in PMSM drives by adjusting the filter parameters to enhance overall performance. Bolognani introduced a streamlined approach to matrix selection, departing from the traditional trial-and-error method. When coupled with a potential novel self-tuning procedure, these matrices aimed to bring the EKF drive closer to a readily available product. Experimental tests conducted on functional prototypes affirmed the effectiveness of the proposed procedures. Loebis et al. [18] explored the adaptive

tuning of a Kalman filter using fuzzy logic for an intelligent Autonomous Underwater Vehicle (AUV) navigation system.

The study aims to adjust Kalman filter parameters dynamically through fuzzy logic, enhancing the navigation system's intelligence and adaptability. This adaptive approach, utilizing fuzzy logic for real-time adjustments, improved AUV navigation across different conditions. Implementation of real experimental data from AUV trials with the Hammerhead AUV showed promising results in improving the estimation of individual Kalman filter types and enhancing the overall accuracy of the integrated INS/GPS.

This paper is organized as follows: Section II details the traditional approach of RISS/GPS integration using the Extended Kalman Filter (EKF) and introduces our novel technique. Section III presents the results of simulations and experimental tests to evaluate the new approach. Finally, Section IV concludes the paper with critical takeaways and future directions.

II. Materials and Method

Inertial sensors, especially those used in lower-cost RISS systems, are prone to errors accumulating over time (drift), which degrade long-term accuracy. To compensate, RISS often relies on external sources like GPS [19], [20], [21]. Kalman filters are ideal for state estimation in linear systems with Gaussian noise, but their performance depends heavily on system linearity. In navigation systems, this is a challenge. The Extended Kalman Filter (EKF) tackles this by linearizing the system around an operating point using a first-order Taylor series expansion (approximation). This approximation has limitations and can impact filter performance Fig. 1.

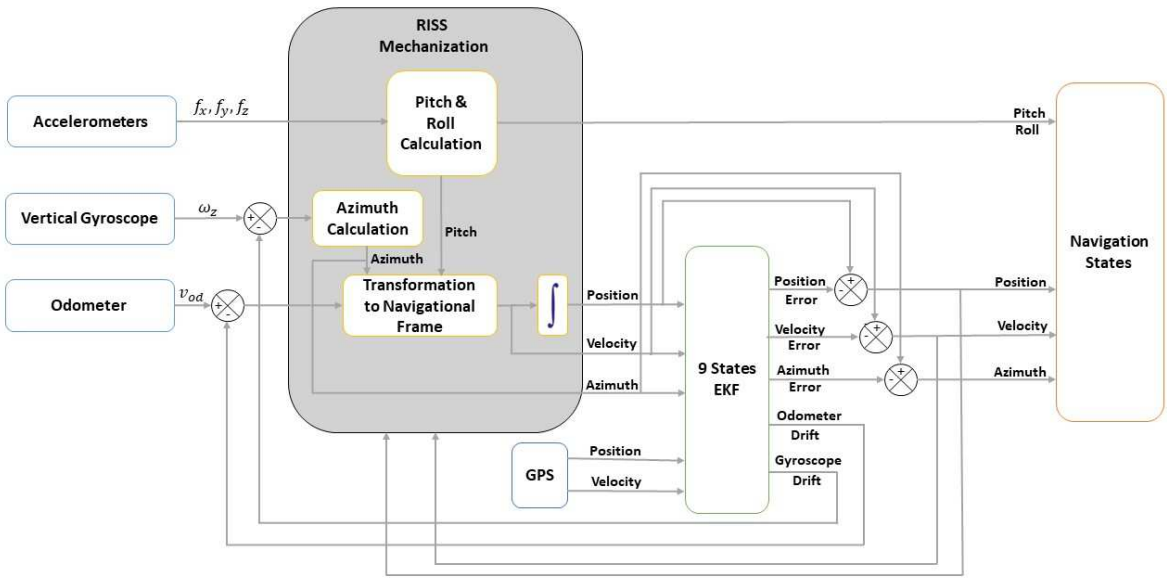

Fig. 1 RISS/GPS Integration using Extended Kalman Filter

The RISS configuration here differs from traditional INS by employing an odometer for speed, calculating pitch and roll from accelerometers instead of gyroscopes, and using a single gyroscope for azimuth. These navigation states are then fused with GPS data within the EKF to refine navigation accuracy. The EKF's outputs are then fed back to improve overall system performance.

A. RISS Mechanization

RISS Mechanization [22], [23] is the process of deducing navigation states (position, velocity, and attitude) from inertial sensor measurements acquired in the body frame. This recursive process depends on the initial conditions, or the previous output combined with new measurements. RISS functions by computing navigation states within the local-level frame. As sensor measurements are acquired in the body frame, a key element of RISS involves deriving the rotation matrix from the body frame to the local-level frame. These navigation states are essential for understanding the platform's movement and orientation in the local-level frame. RISS utilizes information from three accelerometers, one vertical gyroscope, and an odometer to calculate and update these navigation states. Integrating these states enables precise tracking of the platform's position, velocity, and attitude, rendering RISS a dependable navigation solution for scenarios requiring reduced sensor requirements and specific advantages. The RISS mechanization [24] takes a unique approach to navigation.

Unlike traditional systems, it directly calculates pitch and roll angles from accelerometers, cutting the need for integration and minimizing drift. Gyroscope data is used only for azimuth determination, reducing reliance on integration for other parameters. Local-level frame velocity is derived by transforming platform speed measured by the odometer. Finally, these velocities are integrated to compute the system's position. This approach leverages the strengths of both accelerometers and odometers, potentially improving overall accuracy and drift resistance. The dynamic mechanization equations of RISS, as presented in Equation 1, are employed in integrating RISS/GPS, yielding the attitude, velocity, and position in the local level frame. The RISS system is impacted by sensor noise, which leads to output drift. GPS is integrated with RISS to improve performance.

$$\begin{pmatrix} \varphi_t \\ \lambda_t \\ h_t \\ V_t^e \\ V_t^n \\ V_t^{up} \\ p_t \\ r_t \\ A_t \end{pmatrix} = \begin{pmatrix} \varphi_{t-1} + \frac{V_t^n}{R_M+h_t}\Delta t \\ \lambda_{t+1} + \frac{V_t^e}{(R_N+h_t)\cos(\varphi_t)}\Delta t \\ h_{t-1} + V_t^{up}\Delta t \\ V_t^{od}\sin(A_t)\cos(p_t) \\ V_t^{od}\cos(A_t)\cos(p_t) \\ V_t^{od}\sin(p_t) \\ tan^{-1}\left(\frac{-f_t^y}{\sqrt{(f_t^x)^2+(f_t^z)^2}}\right) \\ tan^{-1}\left(\frac{-f_t^x}{f_t^z}\right) \\ A_{t-1} + \left(\omega_t^z - \omega^e\sin(\varphi_t) - \frac{V_t^e\tan(\varphi_t)}{R_N+h_t}\right)\Delta t \end{pmatrix} \quad (1)$$

where

φ, λ, h	: are the curvilinear position (latitude, longitude, and altitude).
V^e, V^n, V^{up}	: are the velocities in east, north, and up direction.
p, r, A	: are the attitude (pitch, roll, and azimuth).
R_M	: represents the meridian radius of curvature of the Earth.
R_N	: represents the normal radius of ellipsoid of the Earth.
V^{od}	: represents the speed measured by the odometer.
f^x, f^y, f^z	: represent the acceleration measurements obtained from three orthogonal accelerometers.
ω^z	: stands for the rotational velocity measured by the vertical gyroscope.
$\omega^e \sin(\varphi)$	: depicts the station component of Earth rotation.
$\frac{V^e \tan(\varphi)}{R_N + h}$	: depicts the non-station component of Earth rotation.

B. Extended Kalman Filter

A common practice is to combine GPS data (position and velocity) with RISS calculations using a closed loop, loosely coupled Kalman Filter (KF) [25], [26]. This filter prioritizes reliable data to minimize the impact of noise in navigation estimates. However, unaided RISS operation suffers from accumulating errors (drift) over time. To address this, error models are crucial for understanding and predicting these errors. Since errors in dynamic systems are constantly changing, they require non-linear equations for description. This led to the development of the EKF, which builds upon the KF by linearizing the system to derive simpler linear equations that effectively manage errors and improve navigation accuracy. Linearization occurs through applying a Taylor series expansion while disregarding higher-order terms. The outcomes produced by the Extended Kalman Filter include position errors (latitude ($\delta\varphi$), longitude ($\delta\lambda$), and altitude (δh)), velocity errors (east velocity (δV^e), north velocity (δV^n), and up velocity (δV^{up})), azimuth (δA), stochastic gyroscope error ($\delta\omega^z$), and errors related to the acceleration derived from the odometer (δod). The simplified position error can be derived as:

$$\begin{pmatrix} \delta\dot{\varphi} \\ \delta\dot{\lambda} \\ \delta\dot{h} \end{pmatrix} = \begin{pmatrix} 0 & \frac{1}{R_M+h} & 0 \\ \frac{1}{(R_N+h)\cos(\varphi)} & 0 & 0 \\ 0 & 0 & 1 \end{pmatrix} \begin{pmatrix} \delta V^e \\ \delta V^n \\ \delta V^{up} \end{pmatrix} \quad (2)$$

The velocity error model is:

$$\begin{pmatrix} \delta\dot{V}^e \\ \delta\dot{V}^n \\ \delta\dot{V}^{up} \end{pmatrix} = \begin{pmatrix} a^{od}\cos(A)\cos(p) & \sin(A)\cos(p) & 0 \\ -a^{od}\sin(A)\cos(p) & \cos(A)\cos(p) & 0 \\ 0 & \sin(p) & 0 \end{pmatrix} \begin{pmatrix} \delta A \\ \delta od \\ \delta\omega^z \end{pmatrix} \quad (3)$$

The azimuth error model as:

$$\delta\dot{A} = \cos(p)\cos(r)\,\delta\omega^z \quad (4)$$

The error model for gyro drift and odometer drift is a stochastic model, and it is advisable to employ the first-order stochastic Gauss-Markov model as follows:

$$\delta\dot{od} = -\gamma\delta od + \sqrt{2\gamma\sigma_{od}^2}W \quad (5)$$

$$\delta\dot{\omega}^z = -\beta\delta\omega^z + \sqrt{2\beta\sigma_{\omega^z}^2}W \quad (6)$$

where γ represents the inverse of the autocorrelation time for odometer-derived noise, σ_{od}^2 denotes the variance of odometer-derived noise, β stands for the inverse of the autocorrelation time for gyroscope noise and $\sigma_{\omega^z}^2$ represents the variance of gyroscope noise.

The variance and the inverse of the correlation times can be derived from the raw measurements. EKF operates in two key stages: prediction and update. The prediction step, detailed in equations 7 and 8, focuses on calculating the anticipated error state and its corresponding uncertainty (covariance matrix) based on the system's previous state and the time elapsed. This essentially forecasts how errors might evolve before incorporating new sensor measurements.

$$\hat{X}_k^- = A\hat{X}_{k-1} \quad (7)$$

$$P_k^- = AP_{k-1}A^T + Q \quad (8)$$

where:

$\hat{X}_k^-$	The prior state vector includes error components associated with position, velocity, azimuth, gyro drift, and odometer.
A	the state transition matrix encompasses the error models outlined in equations 2-6.
P_k^-	Before incorporating new sensor measurements, the prior state error covariance matrix quantifies the uncertainty associated with the predicted error state vector.
Q	is the process noise covariance matrix that quantifies the error in the RISS system.

Following the prediction step, the EKF enters the correction stage outlined in equations 9, 10, and 11. Here, it calculates the Kalman gain, which acts like a control knob, determining how much weight to assign to the new sensor measurements. Based on this gain and the latest sensor data, the EKF updates both the error state vector (refined error estimates) and the error covariance matrix (adjusted uncertainty levels), effectively incorporating fresh information while accounting for potential

measurement noise. This continuous process of prediction and correction allows the EKF to learn and adapt, leading to increasingly accurate navigation estimates.

$$K_k = P_k^- H^T (H P_k^- H^T + R)^{-1} \tag{9}$$

$$\hat{X}_k = \hat{X}_k^- + K_k\left(Z_k - H\hat{X}_k^-\right) \tag{10}$$

$$P_k = (I - K_k H) P_k^- \tag{11}$$

where

- K represents the Kalman gain.
- R represents the uncertainty in GPS readings.
- H represents the measurement model matrix.
- $\hat{X}_k$ The posterior state vector represents the updated error state vector incorporating the latest GPS information.
- P_k A posteriori state error covariance matrix represents the updated uncertainty in the error state vector after incorporating the latest GPS measurements.
- Z signifies the vector of measurements received from the GPS at a specific time step.

The EKF, as described earlier, has some limitations. One issue is its reliance on the state transition matrix (A). This matrix is derived through a Taylor series expansion, essentially creating a linear approximation of the system's behavior. While convenient, this approach disregards higher-order terms, introducing potential inaccuracies in the error estimation of the state vector. Another challenge is the propagation of errors through the system. The EKF's linearization can lead to significant deviations in the mean and covariance of the system state over time. In extreme cases, this may even cause the filter to diverge completely and lose track of the true state.

Furthermore, the EKF depends on two key covariance matrices: measurement noise covariance (R) and process noise covariance (Q). These matrices quantify the uncertainties associated with sensor measurements and the system's dynamics. Though, they are often estimated based on limited initial knowledge, and their accuracy can significantly impact the filter's performance. Inaccuracies in these matrices can lead to imprecise filter state estimates and even filter divergence [27], [28]. The EKF leverages GPS measurements to refine navigation data and mitigate drift. Yet, GPS has limitations. Signal quality can be compromised underwater, indoors, or under dense foliage. Additionally, reflections from buildings or water can cause multipath interference, reducing accuracy. Other electronic devices and radio signals can also interfere. Satellites can be unavailable due to maintenance or maneuvers, and consumer-grade GPS offers lower accuracy than military systems.

Finally, GPS is susceptible to intentional jamming or spoofing, raising security concerns. This paper introduces a new integration method to address these limitations and achieve a robust, high-performance navigation system. Our novel integration method, which tackles the shortcomings of EKF integration, is illustrated in Fig. 2. Firstly, a self-tuning algorithm streamlines filter parameter optimization. Secondly, it incorporates a method to verify GPS signal integrity before integration using a GPS integrity algorithm, eliminating issues caused by misleading data. Lastly, employing the UKF algorithm during integration overcomes the linearization challenges inherent in the EKF, leading to a more robust and accurate navigation system.

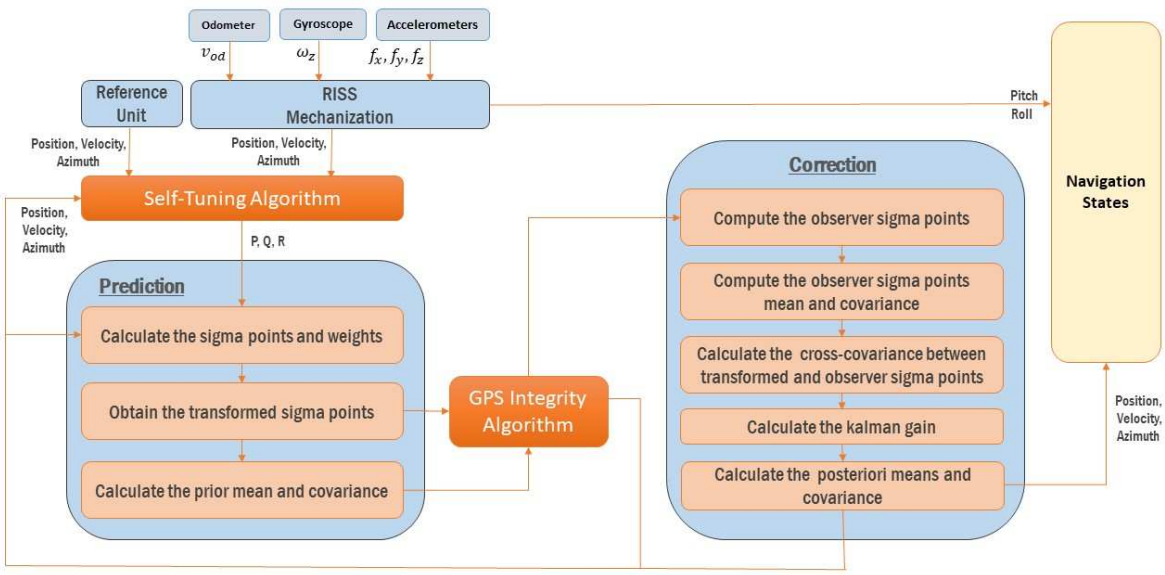

Fig. 2 New RISS/GPS Integration Technique

A. Self-Tuning Algorithm

The self-tuning algorithm refines filter parameters using a three-pronged approach. It leverages: 1) a true reference navigation state from a high-precision reference unit, 2) RISS navigation states derived from the odometer, vertical gyroscope, and accelerometer data (as detailed in equations 1), and 3) the navigation states obtained after RISS and GPS integration. The Q matrix captures the uncertainties associated with errors in the RISS system itself, arising from limitations in the sensors (odometer, gyroscope, accelerometers) used for navigation. These initial uncertainties are derived from the

difference between the ground truth reference state S_{ref} and the raw, uncorrected navigation state data S_{RISS} provided by the RISS system, as shown in equation 12. Essentially, the Q matrix reflects our initial confidence in the RISS data by quantifying the potential discrepancies between the system's raw measurements and the actual solution.

$$Q(i,j) = \begin{Bmatrix} avg(S_{ref} - S_{RISS}), & if\ i = j \\ 0, & otherwise \end{Bmatrix} \quad (12)$$

This initial error assumes the error characteristics in each state (like position and velocity errors) are independent and don't influence each other. Only the diagonal elements of Q (representing individual state uncertainties) have values to reflect this, while off-diagonal elements are set to zero. The Q matrix remains constant during operation. This is because the error characteristics of the RISS system (odometer, gyroscope, accelerometers) are assumed to be relatively stable throughout the operation. The P_0 matrix, representing the initial uncertainty in the filter's output, is based on the error in the navigation state after RISS/GPS integration. This error is calculated as the average difference between the ground truth reference state S_{ref} and the integrated navigation state $S_{RISS/GPS}$ as shown in equation 13.

$$P_0(i,j) = \begin{Bmatrix} avg\left(S_{ref} - S_{\frac{RISS}{GPS}}\right), & if\ i = j \\ 0, & otherwise \end{Bmatrix} \quad (13)$$

Much like the Q matrix, this initial error assumes independence among each state's uncertainty, ensuring they don't affect one another. Consequently, only the diagonal elements of P_0 contain values, with off-diagonal elements set to zero. However, as experiments indicate, initializing P0 with zeros or minimal values can impede the filter's convergence. Fortunately, the P_0 matrix only requires a one-time setup and subsequently updates automatically through the filter's equations as new data is received. The R Matrix serves as a representation of error covariance within the GPS measurements. Typically, GPS modules furnish information regarding error variance or standard deviation for both position and velocity. These received variance values can be directly incorporated into the R matrix, reflecting the confidence level in the GPS readings and accounting for potential influences from outages and interference conditions. As each epoch unfolds, new values are received and seamlessly integrated into the R matrix.

Following the initial establishment of the error covariance matrices (P_0 and Q), a procedure known as error covariance fine-tuning is executed. In this process, these matrices undergo manual adjustments within an iterative loop. The effectiveness of this fine-tuning is commonly assessed through system convergence time, state error covariance matrix behavior, and final estimated state accuracy. Through iterative modifications to P_0 and Q based on these criteria, the error covariance fine-tuning process seeks to enhance the filter's performance, striving for optimal accuracy in navigation estimates.

B. Predication Step

Based on the UKF, the novel algorithm demonstrates superior performance for nonlinear systems compared to the EKF. The UKF employs a sampling approach, representing the system through Gaussian random variables. It initiates by selecting n points from the previous distribution of the random variable, termed sigma points. These points are then propagated through a nonlinear function instead of a linearized one, thereby mitigating errors associated with system linearization. This technique, considering the spread of the random variable, proves more accurate than the Taylor series linearization [29], [30]. Like the EKF, the UKF comprises two primary steps: the prediction step and the correction step, preceded by an additional step for sigma point determination. Fig. 2 depicts the prediction step, initiating with the selection of sigma points using equations 14, 15, and 16.

$$X_{0,k+1} = X_k\,, \quad for\ i = 0 \quad (14)$$

$$X_{i,k+1} = X_k + \left(\gamma\sqrt{P_{xx}}\right)_i, \quad for\ i = 1, \ldots\ldots, n \quad (15)$$

$$X_{i,k+1} = X_k - \left(\gamma\sqrt{P_{xx}}\right)_i, \quad for\ i = n+1, \ldots\ldots, 2n \quad (16)$$

where

- X : signifies the state vector means, encompassing position, velocity, azimuth and sensors error information at a specific time step
- P_{xx} : represents the uncertainty associated with the state vector.
- $\left(\gamma\sqrt{P_{xx}}\right)_i$: The ith row of the matrix holds the square root information for the corresponding row of the original matrix, calculated via Cholesky factorization
- n : represents the number of elements in the state vector.

P_{xx} representing the initial uncertainty in the system's state is defined by equation 13. The weights for each sigma point in the UKF are determined based on the prior mean and covariance, calculated using equations 17, 18, and 19 [31].

$$W_0^m = \frac{\lambda}{n+\lambda} \quad (17)$$

$$W_0^c = \frac{\lambda}{n+\lambda}(1 - \alpha^2 + \beta) \quad (18)$$

$$W_i^m = W_i^c = \frac{1}{2(n+\lambda)} \quad (19)$$

where

- α : controls the spread of sigma points in the filter, allowing for tighter clustering around the mean (smaller values) or a more comprehensive exploration of the state space (larger values). Its range typically falls between 10 −4 and 1.
- β : acts as a scaling factor, adjusting the spread of sigma points based on prior knowledge of the distribution of a variable. A common value of 2 for Gaussian distributions ensures efficient sigma point selection.

Equations 20 and 21 define λ and γ

$$\lambda = \alpha^2(n + k) - n \quad (20)$$

$$\gamma = \sqrt{n + \lambda} \quad (21)$$

The filter's scaling parameter k, typically set to zero, controls the influence of higher-order terms (beyond mean and covariance) during non-linear transformations. The filter propagates sigma points through the non-linear navigation system model illustrated in equation 1 to obtain transformed points and then computes the prior mean and covariance using equations 22 and 23.

$$\hat{X}_{k+1} = \sum_{i=0}^{2n} W_i^m X_{i,k+1} \quad (22)$$

$$P_{xx,k+1} = Q + \sum_{i=0}^{2n} W_i^c \left[X_{i,k+1} - \hat{X}_{k+1}\right]\left[X_{i,k+1} - \hat{X}_{k+1}\right]^T \quad (23)$$

The Q matrix captures the initial uncertainties in the RISS navigation system due to sensor errors, calculated as in equation 12.

C. GPS Integrity Algorithm

The proposed technique tackles the issue of misleading GPS signals caused by blockage and interference. To ensure reliable navigation, it incorporates a GPS integrity algorithm. This algorithm operates in a waiting loop for new GPS measurements and then validates their reliability before incorporating them into the filter's correction step. As defined in equation 24, validation considers two factors: 1) the change between consecutive GPS readings, which should be limited due to the car's motion, and 2) the discrepancy between predicted navigation states and current GPS data, which should be small due to well-calibrated sensors. If either difference surpasses a threshold, the GPS measurement is deemed unreliable and discarded, preventing such errors from affecting the filter's performance.

$$\begin{aligned} &\left|RISS_{predicted,k+1} - GPS_{measurements,k+1}\right| \\ &\qquad > TH_{RISS} \quad or \\ &\left|GPS_{measurements,k+1} - GPS_{measurements,k}\right| \\ &\qquad > TH_{GPS} \end{aligned} \quad (24)$$

where TH_{RISS} and TH_{GPS} are manual tuning to achieve the highest possible performance.

D. Correction Step

The technique then incorporates the measurement update by passing the transformed sigma points through the observer function h, resulting in the Y sigma points.

$$Y_{i,k+1} = h\left(X_{i,k+1}\right) \quad (25)$$

Following that, the mean and covariance of the observer sigma points are calculated.

$$\hat{Y}_{k+1} = \sum_{i=0}^{2n} W_i^m Y_{i,k+1} \quad (26)$$

$$P_{yy,k+1} = R + \sum_{i=0}^{2n} W_i^c \left[Y_{i,k+1} - \hat{Y}_{k+1}\right]\left[Y_{i,k+1} - \hat{Y}_{k+1}\right]^T \quad (27)$$

The algorithm then computes the cross-covariance between the predicted sigma points and the observer sigma points.

$$P_{xy,k+1} = \sum_{i=0}^{2n} W_i^c \left[X_{i,k+1} - \hat{X}_{k+1}\right]\left[Y_{i,k+1} - \hat{Y}_{k+1}\right]^T \quad (28)$$

The Kalman gain is subsequently calculated as follows:

$$K_{k+1} = \frac{P_{xy}}{P_{yy}} \quad (29)$$

Finally, the algorithm updates the state estimate by computing the posterior mean and covariance.

$$X_{i,k+1} = \hat{X}_{k+1} + K_{k+1}\left[Z_{k+1} - \hat{Y}_{k+1}\right] \quad (30)$$

$$P_{XX,k+1} = P_{xx,k+1} - K_{k+1} P_{yy,k+1} (K_{k+1})^T \quad (31)$$

Z_{k+1} represents the GPS measurements, and the new technique significantly improves performance compared to the EKF, as demonstrated in the experimental results section.

III. Results and Discussion

The experiment simulation leveraged two datasets collected at 20 Hz from a VTI SCC1300-D04 MEMS-based IMU unit. Vehicle speed data was acquired via a CarChip data logger connected to the car's OBD-II interface, with GPS updates received every second. The navigation states estimated using these sensor measurements were compared against a reference trajectory provided by a high-end Novatel SPAN unit. This comparison assessed the new algorithm's performance against the traditional EKF. Fig. 3 depicts the navigation trajectories obtained from the Novatel SPAN unit (ground truth), standalone RISS (uncorrected), RISS/GPS integration with EKF, and finally, RISS/GPS integration using the proposed algorithm.

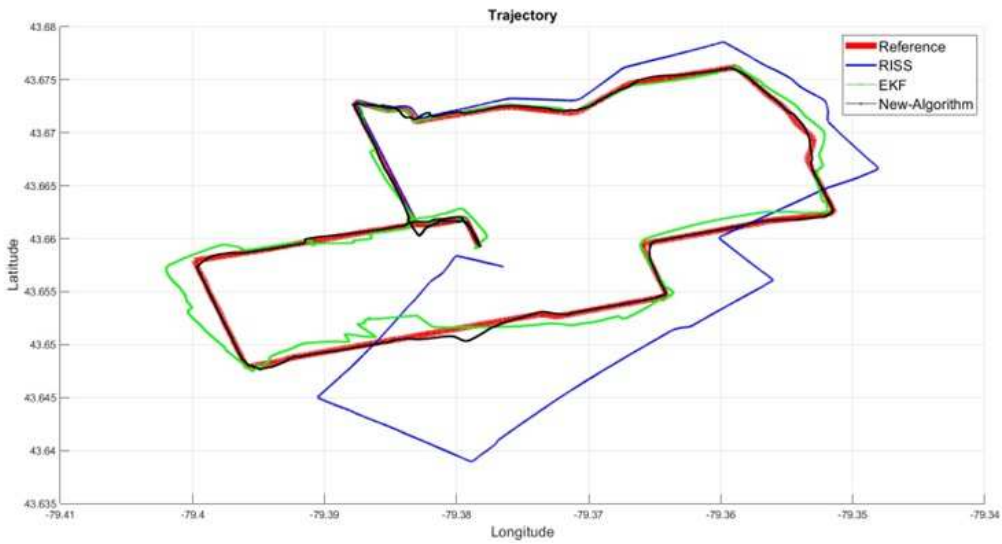

Fig. 3 Trajectory1 RISS/EKF/New-Algorithm Results

Fig. 4 depicts deviations from each system's true position, highlighting the new technique's superior performance over the EKF. Fig. 5 and Fig. 6 evaluate the velocity performance of both systems: Fig. 5 compares their estimated velocities to the reference system, while Fig. 6 depicts the corresponding velocity errors.

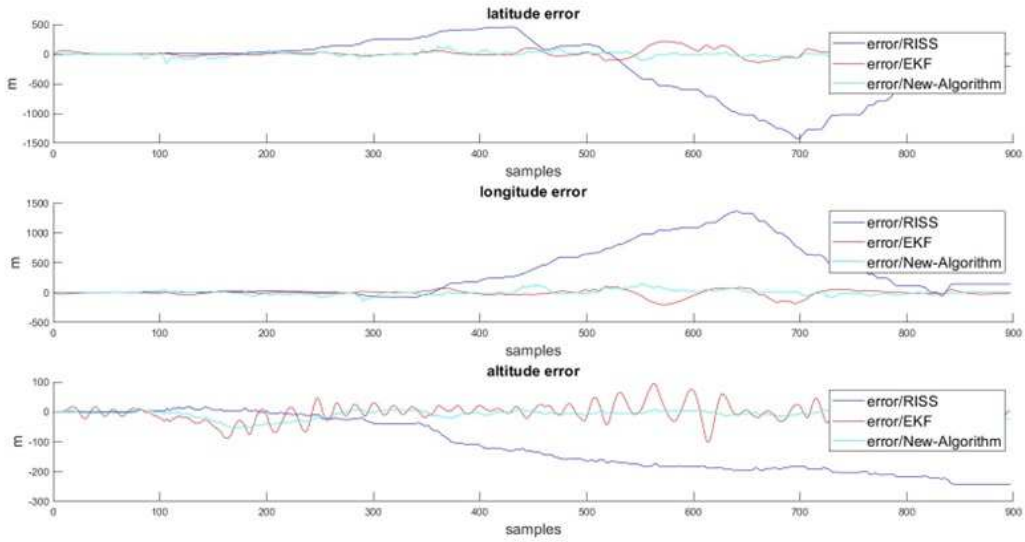

Fig. 4 Trajectory1 RISS/EKF/New-Algorithm Position Errors

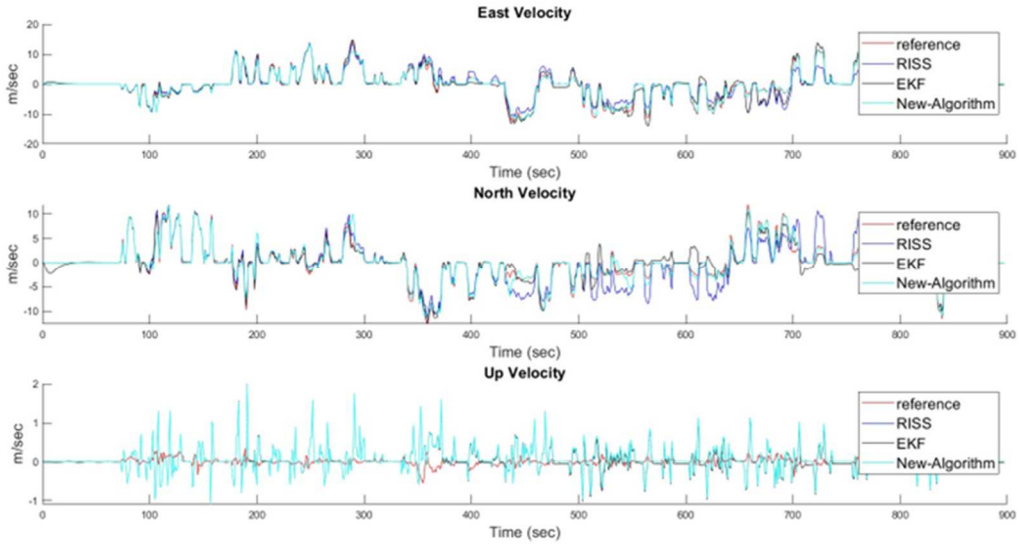

Fig. 5 Trajectory1 RISS/EKF/New-Algorithm Velocity Results

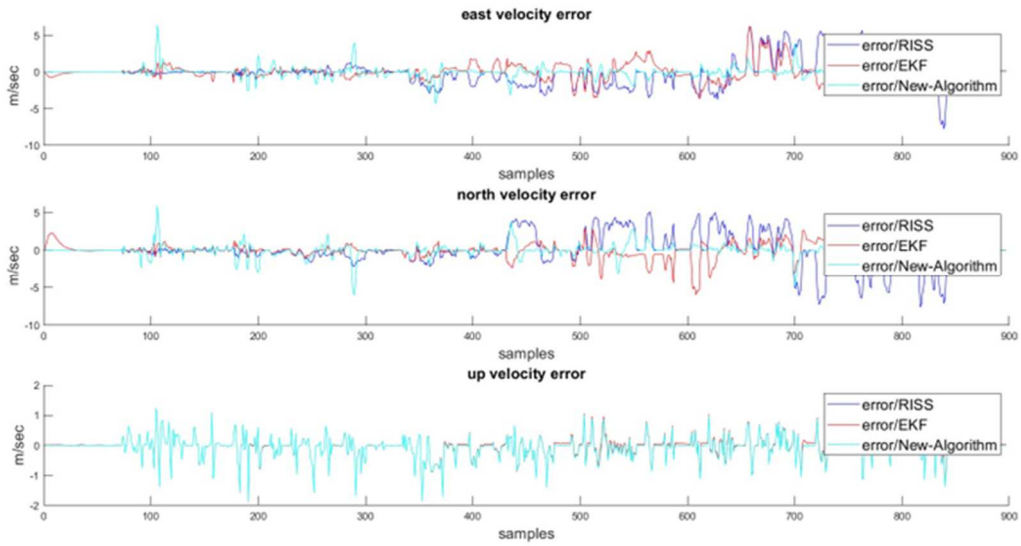

Fig. 6 Trajectory1 RISS/EKF/New-Algorithm Velocity Errors

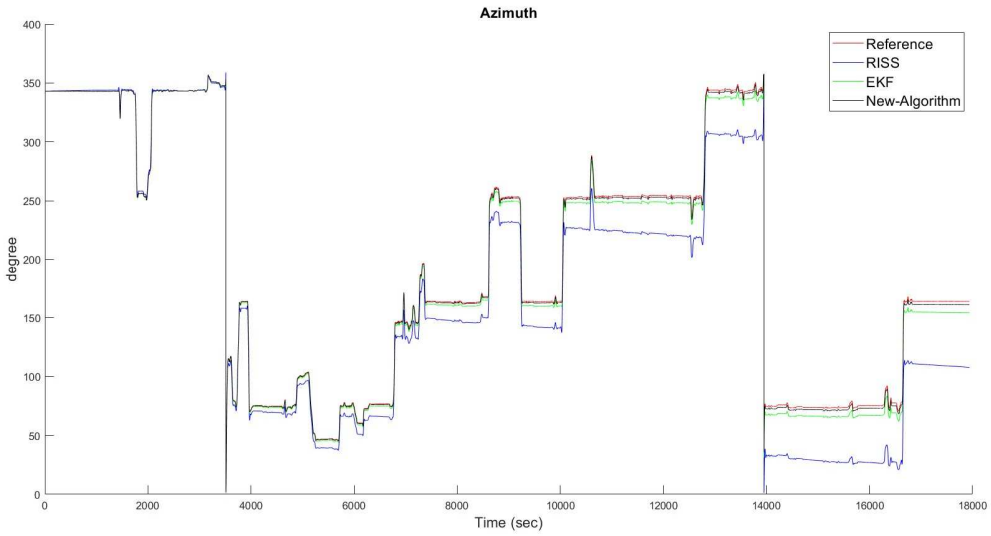

Fig. 7 Trajectory1 RISS/EKF/New-Algorithm Azimuth Results

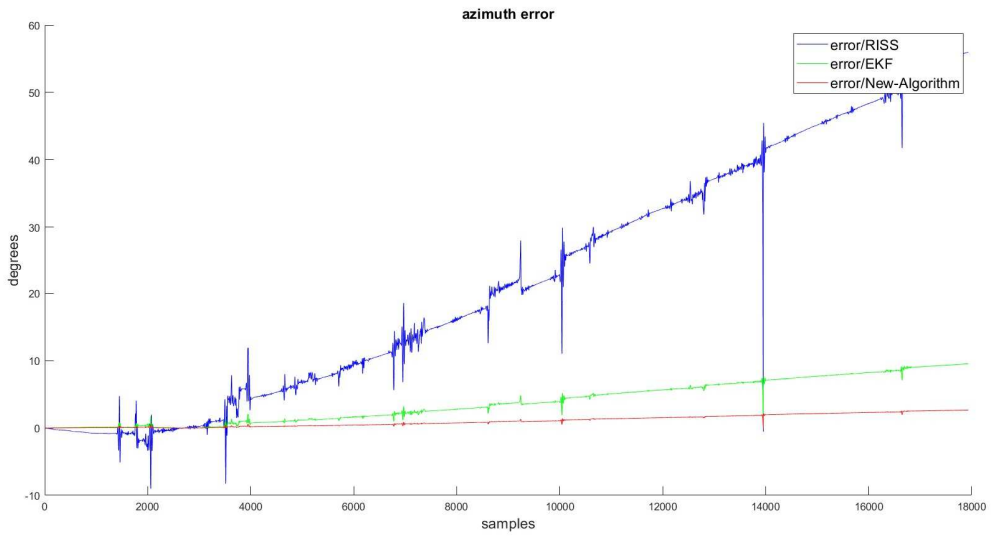

Fig. 8 Trajectory1 RISS/EKF/New-Algorithm Azimuth Errors

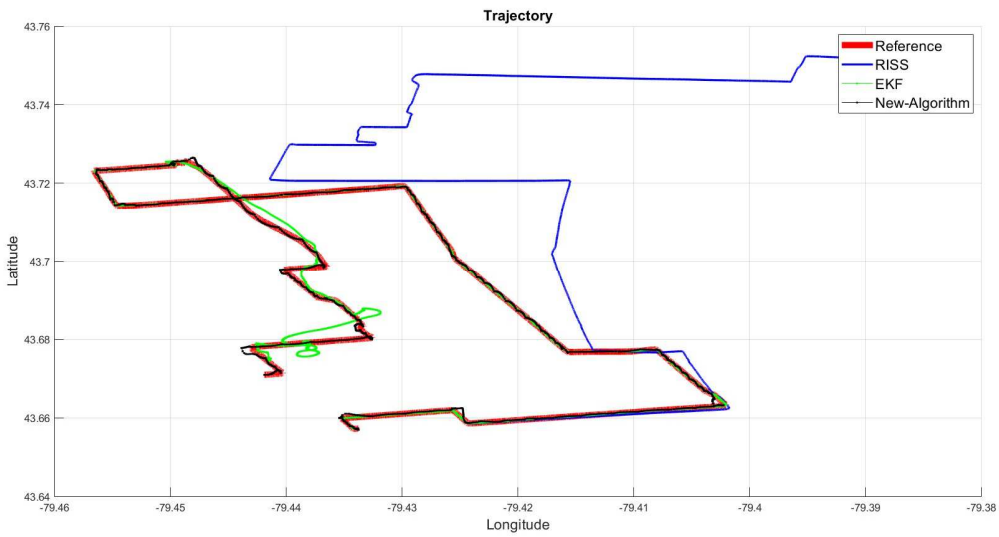

Fig. 9 Trajectory2 RISS/EKF/New-Algorithm Results

Fig. 7 and Fig. 8 showcase the azimuth accuracy of the systems, with Fig. 7 presenting the estimated azimuth and Fig. 8 illustrating the corresponding azimuth errors. Fig. 9 visually showcases the enhanced performance of the proposed technique with another dataset, comparing trajectories of the standalone RISS, RISS/GPS integration with EKF, and RISS/GPS integration with the new algorithm against a reference path. The new method distinctly generates a smoother and more accurate trajectory. Additionally, Table III quantifies this improvement by presenting the RMSE for position, velocity, and azimuth, underscoring the notable reduction in errors achieved by the proposed technique compared to EKF-based integration.

Table II summarizes the maximum Root Mean Square Error (RMSE) values for various navigation states, highlighting the performance improvement achieved by the new technique compared to the EKF integration method.

TABLE II
TRAJECTORY1 EKF/NEW-ALGORITHM RMSE COMPARISON

RMSE	EKF	New-Algorithm
Azimuth	5.0632°	1.4119°
East Velocity	1.2182 m/s	0.6299 m/s
North Velocity	1.6721 m/s	0.7553 m/s
Up Velocity	0.3549 m/s	0.3532 m/s
Latitude	82.9741 m	36.2292 m
Longitude	74.8394 m	48.747 m
Longitude	32.8003 m	7.7789 m

TABLE III
TRAJECTORY2 EKF/NEW-ALGORITHM RMSE COMPARISON

RMSE	EKF	New-Algorithm
Azimuth	103.3814°	45.8807°
East Velocity	2.9956 m/s	1.7161 m/s
North Velocity	5.276 m/s	1.9267 m/s
Up Velocity	0.2626 m/s	0.1981 m/s
Latitude	270.9458 m	69.8641 m
Longitude	98.6208 m	42.8605 m
Longitude	17.825 m	4.7636 m

IV. CONCLUSION

This paper proposes a new integration method for RISS/GPS systems that surpasses the performance of the traditional EKF-based RISS/GPS approach. This improvement stems from three key advancements: 1) a self-tuning algorithm that optimizes convergence time, prevents potential divergence issues, and ultimately enhances overall accuracy. 2) A GPS integrity algorithm that ensures the correction step utilizes only reliable GPS measurements determined by user-defined thresholds for optimal performance. 3) The UKF implementation effectively handles the non-linearities inherent in the navigation system model, unlike the EKF's linearization approach using a first-order Taylor series expansion. To evaluate this new algorithm, we compared it against the EKF method using two datasets collected from a VTI SCC1300-D04 IMU unit. A high-precision Novatel SPAN unit provided the reference ground truth for comparison. The results presented in the paper conclusively demonstrate that the proposed algorithm significantly improves navigation performance compared to the EKF for both datasets.

ACKNOWLEDGMENT

We extend our heartfelt appreciation to Dr. Aboelmagd Noureldin from the Royal Military College of Canada, for graciously providing the dataset utilized in this experiment. His contribution was indispensable to our research, and we deeply value his support.

REFERENCES

[1] A. Noureldin, T. B. Karamat, and J. Georgy, Fundamentals of Inertial Navigation, Satellite-based Positioning and their Integration. Springer Berlin Heidelberg, 2013. doi: 10.1007/978-3-642-30466-8.

[2] N. El-Sheimy and A. Youssef, "Inertial sensors technologies for navigation applications: state of the art and future trends," Satellite Navigation, vol. 1, no. 1, Jan. 2020, doi: 10.1186/s43020-019-0001-5.

[3] Y. Liu, X. Fan, C. Lv, J. Wu, L. Li, and D. Ding, "An innovative information fusion method with adaptive Kalman filter for integrated INS/GPS navigation of autonomous vehicles," Mechanical Systems and Signal Processing, vol. 100, pp. 605–616, Feb. 2018, doi:10.1016/j.ymssp.2017.07.051.

[4] E. S. Abdolkarimi and M.-R. Mosavi, "A low-cost integrated MEMS-based INS/GPS vehicle navigation system with challenging conditions based on an optimized IT2FNN in occluded environments," GPS Solutions, vol. 24, no. 4, Aug. 2020, doi: 10.1007/s10291-020-01023-9.

[5] I. P. Prikhodko, B. Bearss, C. Merritt, J. Bergeron, and C. Blackmer, "Towards self-navigating cars using MEMS IMU: Challenges and opportunities," 2018 IEEE International Symposium on Inertial Sensors and Systems (INERTIAL), pp. 1–4, Mar. 2018, doi:10.1109/isiss.2018.8358141.

[6] A. Abosekeen, A. Noureldin, and M. J. Korenberg, "Improving the RISS/GNSS Land-Vehicles Integrated Navigation System Using Magnetic Azimuth Updates," IEEE Transactions on Intelligent Transportation Systems, vol. 21, no. 3, pp. 1250–1263, Mar. 2020, doi:10.1109/tits.2019.2905871.

[7] N. Li, L. Guan, Y. Gao, Z. Liu, Y. Wang, and H. Rong, "A Low Cost Civil Vehicular Seamless Navigation Technology Based on Enhanced RISS/GPS between the Outdoors and an Underground Garage," Electronics, vol. 9, no. 1, p. 120, Jan. 2020, doi:10.3390/electronics9010120.

[8] F. Wu, H. Luo, H. Jia, F. Zhao, Y. Xiao, and X. Gao, "Predicting the Noise Covariance With a Multitask Learning Model for Kalman Filter-Based GNSS/INS Integrated Navigation," IEEE Transactions on Instrumentation and Measurement, vol. 70, pp. 1–13, 2021, doi:10.1109/tim.2020.3024357.

[9] R. Van Der Merwe and E. A. Wan, "Sigma-Point Kalman Filters for Integrated Navigation," 1995.

[10] R. V. Garcia, P. C. P. M. Pardal, H. K. Kuga, and M. C. Zanardi, "Nonlinear filtering for sequential spacecraft attitude estimation with real data: Cubature Kalman Filter, Unscented Kalman Filter and Extended Kalman Filter," Advances in Space Research, vol. 63, no. 2, pp. 1038–1050, Jan. 2019, doi: 10.1016/j.asr.2018.10.003.

[11] D. Sabzevari and A. Chatraei, "INS/GPS Sensor Fusion based on Adaptive Fuzzy EKF with Sensitivity to Disturbances," IET Radar, Sonar & Navigation, vol. 15, no. 11, pp. 1535–1549, Jun. 2021, doi: 10.1049/rsn2.12144.

[12] D. M.G. and A. Arun, "Analysis of INS Parameters and Error Reduction by Integrating GPS and INS Signals," 2018 International Conference on Design Innovations for 3Cs Compute Communicate Control (ICDI3C), pp. 18–23, Apr. 2018, doi: 10.1109/icdi3c.2018.00013.

[13] T. D. Powell, "Automated Tuning of an Extended Kalman Filter Using the Downhill Simplex Algorithm," Journal of Guidance, Control, and Dynamics, vol. 25, no. 5, pp. 901–908, Sep. 2002, doi: 10.2514/2.4983.

[14] K. A. Myers and B. D. Tapley, "Adaptive Sequential Estimation with Unknown Noise Statistics," 1976.

[15] P. Matisko and V. Havlena, "Noise covariance estimation for Kalman filter tuning using Bayesian approach and Monte Carlo," International Journal of Adaptive Control and Signal Processing, vol. 27, no. 11, pp. 957–973, Dec. 2012, doi: 10.1002/acs.2369.

[16] D.-J. Lee and K. T. Alfriend, "Adaptive Sigma Point Filtering for State and Parameter Estimation," 2004.

[17] S. Bolognani, L. Tubiana, and M. Zigliotto, "Extended kalman filter tuning in sensorless PMSM drives," IEEE Transactions on Industry

Applications, vol. 39, no. 6, pp. 1741–1747, Nov. 2003, doi:10.1109/tia.2003.818991.

[18] D. Loebis, R. Sutton, J. Chudley, and W. Naeem, "Adaptive tuning of a Kalman filter via fuzzy logic for an intelligent AUV navigation system," Control Engineering Practice, vol. 12, no. 12, pp. 1531–1539, Dec. 2004, doi: 10.1016/j.conengprac.2003.11.008.

[19] M. Elsheikh, A. Noureldin, and M. Korenberg, "Integration of GNSS Precise Point Positioning and Reduced Inertial Sensor System for Lane-Level Car Navigation," IEEE Transactions on Intelligent Transportation Systems, vol. 23, no. 3, pp. 2246–2261, Mar. 2022, doi:10.1109/tits.2020.3040955.

[20] M. Karaim, M. Tamazin, and A. Noureldin, "An Efficient Ultra-Tight GPS/RISS Integrated System for Challenging Navigation Environments," Applied Sciences, vol. 10, no. 10, p. 3613, May 2020, doi: 10.3390/app10103613.

[21] A. Aboutaleb, A. S. El-Wakeel, H. Elghamrawy, and A. Noureldin, "LiDAR/RISS/GNSS Dynamic Integration for Land Vehicle Robust Positioning in Challenging GNSS Environments," Remote Sensing, vol. 12, no. 14, p. 2323, Jul. 2020, doi: 10.3390/rs12142323.

[22] Y. Gao, Z. Liu, Y. Wang, and A. Noureldin, "A Hybrid RISS/GNSS Method During GNSS Outage in the Land Vehicle Navigation System," IEEE Sensors Journal, vol. 23, no. 8, pp. 8690–8702, Apr. 2023, doi:10.1109/jsen.2023.3257046.

[23] N. Li, Y. Gao, L. Guan, and M. Wu, "A Low-cost Underground Garage Real-time Navigation Algorithm based on the RISS and GPS System," 2020 Chinese Control And Decision Conference (CCDC), pp. 533–538, Aug. 2020, doi: 10.1109/ccdc49329.2020.9164768.

[24] A. Abosekeen, U. Iqbal, A. Noureldin, and M. J. Korenberg, "A Novel Multi-Level Integrated Navigation System for Challenging GNSS Environments," IEEE Transactions on Intelligent Transportation Systems, vol. 22, no. 8, pp. 4838–4852, Aug. 2021, doi:10.1109/tits.2020.2980307.

[25] U. Iqbal, A. Noureldin, J. Georgy, and M. J. Korenberg, "Application of System Identification Techniques for Integrated Navigation," 2020 International Conference on Communications, Signal Processing, and their Applications (ICCSPA), pp. 1–6, Mar. 2021, doi:10.1109/iccspa49915.2021.9385723.

[26] M. Karaim, M. Tamazin, and A. Noureldin, "An Efficient Ultra-Tight GPS/RISS Integrated System for Challenging Navigation Environments," Applied Sciences, vol. 10, no. 10, p. 3613, May 2020, doi: 10.3390/app10103613.

[27] Q. Xu, X. Li, and C.-Y. Chan, "Enhancing Localization Accuracy of MEMS-INS/GPS/In-Vehicle Sensors Integration During GPS Outages," IEEE Transactions on Instrumentation and Measurement, vol. 67, no. 8, pp. 1966–1978, Aug. 2018, doi:10.1109/tim.2018.2805231.

[28] G. Hu, B. Gao, Y. Zhong, and C. Gu, "Unscented kalman filter with process noise covariance estimation for vehicular ins/gps integration system," Information Fusion, vol. 64, pp. 194–204, Dec. 2020, doi:10.1016/j.inffus.2020.08.005.

[29] S. Liu, Z. Wang, Y. Chen, and G. Wei, "Protocol-Based Unscented Kalman Filtering in the Presence of Stochastic Uncertainties," IEEE Transactions on Automatic Control, vol. 65, no. 3, pp. 1303–1309, Mar. 2020, doi: 10.1109/tac.2019.2929817.

[30] G. Hu, L. Ni, B. Gao, X. Zhu, W. Wang, and Y. Zhong, "Model Predictive Based Unscented Kalman Filter for Hypersonic Vehicle Navigation With INS/GNSS Integration," IEEE Access, vol. 8, pp. 4814–4823, 2020, doi: 10.1109/access.2019.2962832.

[31] G. A. Terejanu, "Unscented kalman filter tutorial", University Buffalo, Buffalo 2011.